BBA - General Subjects 1863 (2019) 1560–1567

Contents lists available at ScienceDirect

BBA - General Subjects

journal homepage: www.elsevier.com/locate/bbagen

An atomistic view of the YiiP structural changes upon zinc(II) binding

Davide Sala[a], Andrea Giachetti[b], Antonio Rosato[a,b,c,*]

[a] Magnetic Resonance Center (CERM), University of Florence, Tuscany, Sesto Fiorentino, Italy
[b] Consorzio Interuniversitario di Risonanze Magnetiche di Metallo Proteine, Tuscany, Sesto Fiorentino, Italy
[c] Department of Chemistry, University of Florence, Tuscany, Sesto Fiorentino, Italy

ARTICLE INFO

Keywords:
Zinc transporter
Metal transport
Metal homeostasis
CDF
Cation diffusion

ABSTRACT

Background: YiiP is a bacterial zinc-for-proton antiporter belonging to the cation diffusion facilitator family. The zinc(II) ions are transported across the cell membrane, from the cytosol to the extracellular space.
Methods: We performed atomistic molecular dynamics simulations of the YiiP dimer with zinc(II) ions in solution to elucidate how the metal ions interact with the protein while moving from the cytosol to the transport site.
Results: We observed that of the two cavities of the dimer, only one was accessible from the cytosol during transport. Zinc(II) binding to D49 of the transport site triggered a rearrangement of the transmembrane domain that closed the accessible cavity. Finally, we analyzed the free-energy profiles of metal transit in the channel and observed the existence of a high barrier preventing release from the transport site.
Conclusions: The observed dynamics is consistent with the dimer-dimer interface forming a stable scaffold against which the rest of the trans-membrane rearranges.
General significance: Zinc(II) transporters are present in all kingdoms of life. The present study highlights structural features that might be of general relevance.

1. Introduction

Zinc is the second most abundant trace element in all living organisms and plays a fundamental role in many biological processes [1,2]. Despite sufficient intracellular zinc(II) concentration is needed to supply proteins that require zinc(II) ions as cofactor, intracellular concentrations higher than few hundred picomolar produce cytotoxic effects [3,4]. Therefore, the cellular uptake and the efflux of zinc(II) ions are tightly controlled by specific systems, present at all phylogenetic levels, to maintain its concentration in a quite narrow range [5–7]. In mammals, the Zrt-, Irt-related proteins (ZIPs/Slc39s) are responsible of the uptake of zinc(II) ions into the cell [8,9]. On the contrary, the zinc transporters of the Cation Diffusion Facilitator (CDF) superfamily (ZnTs/Slc30) mediate zinc(II) removal from the cytoplasm into the extracellular space or into intracellular compartments such as secretory vesicles [10–14]. Presently, there is no direct experimental information on the three-dimensional structure of any member of the human ZnT family [15,16]. However, this limit is partially compensated by a relatively well-characterized bacterial homolog, the YiiP transporter from *Escherichia coli* [17,18]. Among the human homologs of YiiP, Znt8 has received significant attention owing to the involvement of its W325R common variant in the onset of type-1 and type-2 diabetes [19–22].

YiiP is a cation-proton antiporter catalysing the efflux of zinc(II) against the uptake of a proton with a 1:1 exchange stoichiometry [23]. YiiP can transport several divalent metal cations but only zinc(II) and cadmium(II) with high efficiency [24]. The first X-ray structure of this transporter was solved in the outward-facing conformation [25]; in 2009 a new structure with better resolution became available (PDB ID: 3H90) [26]. These crystal structures featured an architecture shared among all CDF transporters consisting in a transmembrane domain (TMD) connected to a C-terminal, cytoplasmic domain (CTD). YiiP is a Y-shaped homodimer with six TM helices per monomer clustered in a four-helix bundle (TM1–TM2–TM4–TM5) and a helix pair (TM3–TM6). The TM3-TM6 helix pair provides the dimer interface and protrudes in the cytosolic region. Each YiiP protein chain harbours three zinc(II) binding sites (A-C). Site A is located close to the middle of the TMD and constitutes the tetrahedral zinc(II) transport site, involving D45 and D49 of TM2 as well as H153 and D157 of TM5 [24]. The CTD hosts the C sites in which the binding of two zinc(II) ions enhances the stability of

Abbreviations: CDF, Cation Diffusion Facilitator; TMD, transmembrane domain; CTD, cytosolic domain; EC, extracellular; IC, intracellular; TM, transmembrane; PCA, principal component analysis

* Corresponding author at: Magnetic Resonance Center (CERM), University of Florence, Tuscany, Sesto Fiorentino, Italy.
E-mail address: rosato@cerm.unifi.it (A. Rosato).

https://doi.org/10.1016/j.bbagen.2019.06.001
Received 19 February 2019; Received in revised form 28 May 2019; Accepted 3 June 2019
Available online 06 June 2019

the dimer [26]. The function of site B is unclear. The inward-facing state of the YiiP homolog from *Shewanella oneidensis* (PDB ID: 3J1Z) was solved at 13 Å by cryo-electron microscopy [27]. Based on the comparison of all available structures, it has been proposed that the transport of zinc(II) involves a so-called alternating mechanism [28]. This proposed mechanism involves an allosteric connection between sites A and C through which a zinc(II) ion binding in the C site can promote metal binding and transport to the TMD thanks to the reorientation of the TM3-TM6 helix pair [26]. In turn, the binding of the zinc(II) ion in the transport site A triggers the conformational switch from the inward- to the outward-facing state facilitating the release of zinc(II). Recently, a variation of the alternating mechanism has been proposed in which the motion of the four-helix bundle relative to the static TM3-TM6 scaffold is proposed to be the critical step for the zinc (II) transfer across the membrane [29]. This mechanism relies on a persistent dimer interface within the lipid membrane acting as a static scaffold versus a mobile transport domain; a similar strategy is used also by other secondary active transporters [30]. In this regard, the zinc (II) translocation to the transport site depends on the accessibility of the hydrophobic cavity located in the TMD region facing the intracellular space [31].

In this work, we investigated the zinc-induced dynamics of YiiP from *Escherichia coli* by performing atomistic MD simulations of the inward-facing conformation in presence and without zinc(II) ions in solution, respectively. Our results pointed out how the binding of one zinc(II) ion in the transport site triggers the closing of the portion of the channel going from the cytosolic space to the transport site itself, hereafter called the TM cavity. The TM cavity closing was mainly the result of TM4-TM5 of the four-helix bundle moving towards TM3-TM6. In this regard, TM5 played a crucial role through a reorientation that brought the side chains of L152 and M197 in close contact, thus forming a hydrophobic gate as proposed by Gupta et al. Unexpectedly, we observed that zinc(II) binding triggered the selective opening of only one channel out of the two protein chains in the dimer. Our work provides a detailed view of the mechanism of zinc(II) permeation from the cytosol to the TM cavity and gives hints on the subsequent steps of the transport mechanism.

2. Methods

The dimeric model of the inward-facing state of YiiP from *Escherichia coli* was built with the Modeller software [32] (mod9v2) exploiting two different structural templates. Since the inward- and the outward-facing state share the same conformation of the CTDs, we used the structure with the highest resolution available (PDB ID: 3H90) [26] to model the residues in the range 208–290. Instead, the inward-facing TMDs, spanning residues 7-207, were modelled on the cryo-EM structure of the homologous *Shewanella oneidensis* protein (PDB ID: 3J1Z) [27]. The membrane builder module of the CHARMM-GUI was used to embed the protein in a rectangular lipid bilayer composed by 366 DPPC phospholipids [33,34]. The system was solvated with TIP3P water molecules with a hydration ratio of 1:100 lipid to water. Two dummy atoms were bound with harmonic restraints to the two cytosolic binding sites (site C) to mimic the binuclear zinc coordination mediating the interaction between the CTDs [12]. All the histidine residues were kept neutral. The Nδ-protonated tautomer was used for all the histidine residues of the zinc(II) binding sites that coordinate the metal with the Nε atom in the 3H90 crystal structure. Instead, the Nε-protonated tautomer was used for all the remaining histidine side chains.

The holo-simulations were performed in the presence of 0.150 M $ZnCl_2$ corresponding to 94 zinc(II) ions and 174 (188 minus 14 ions to balance the negative charge of the protein) chloride(I) ions in solution. The non-bonded parameters for zinc(II) were taken in agreement with the use of TIP3P water model in combination with the classical 12-6 LJ non-bonded model [35]. In particular, the Compromise set (CM) of parameters for divalent ions was used (available from the frcmod.ions234lm_126_tip3p file of the AMBER18 package).

The No-zinc simulation was prepared by adding 0.150 M of NaCl corresponding to 104 sodium(I) ions and 90 chloride(I) ions in solution. A harmonic potential was applied to prevent the insertion of sodium(I) ions in the TM cavities.

The E79A simulation was prepared starting from the snapshot of the Holo02 run at 50 ns, when the zinc(II) was already bound to D150 and E79. After introducing the E79A mutation, a chloride(I) ion was added to the system to balance the charge.

All the simulations exploited the same force fields for the lipid and the protein portions of the system, the Amber LIPID17 and the Amber ff14SB, respectively [36,37]. All the calculations were performed with the AMBER Molecular Dynamics Package using the pmemd software [38,39], with the same equilibration protocol. An initial minimization step was carried out using the Steepest Descent algorithm followed by Conjugate Gradient. Langevin dynamics with a collision frequency of 1 ps^{-1} was used to linearly heat the system in constant volume for 1 ns, during which the protein and the ions are restrained with a force constant of 10 kcal/mol/$Å^2$. The equilibrium temperature was set to 323 K, a value commonly used to overcome the phase transition (liquid to gel) temperature of the pure DPPC lipid membrane (about 315 K) [40]. The physiological density of the system was achieved by carrying out an NPT simulation in which the anisotropic pressure scaling is controlled by the Berendsen barostat (pressure relaxation time of 2 ps). Covalently bonded hydrogen atoms were constrained with the SHAKE and SETTLE (for water molecules) algorithms. The PME method with a cutoff of 10 Å was applied to compute electrostatic interactions. The production runs were performed on Nvidia Pascal Xp GPGPU in the same NVT conditions reported above for the heating step [41]. The RMSD of the protein Cα atoms from the starting conformation was calculated over time to check the convergence of the simulations (Fig. S1).

We carried out umbrella sampling simulations using a harmonic biased potential along the zinc(II) diffusion pathway through the TM cavity of the channel [42]. We prepared two runs using a zinc(II) ion as probe and a third run using a sodium(I) ion. The starting structure of the simulations was chosen from the unbiased holo-trajectory when the zinc(II) ion is at the entrance of the TM cavity facing the IC space. In the calculation using the sodium(I) probe, the metal ion was moved some angstroms away from the channel entrance in order to probe also the energetics for its approach to the channel. The metal probes were pulled towards a water molecule fixed by tight distance restraints outside the top exit of the channel. In this way the ion probe is forced to cross the whole TM portion of the transporter. The water molecule was restrained to the Cα of six residues (L22, L58, L95, L131, L152 and L191) located in a stable position in the middle of TM1, TM2, TM3, TM4, TM5 and TM6, respectively. The force constant used to fix the water molecule was 20 kcal/mol/$Å^2$. Instead, the metal probe was pushed through the channel with a force constant of 15 kcal/mol/$Å^2$. The total distance was split in windows of 0.2 Å, each one sampled for 1 ns. The resulting trajectories were computed using the weighted histogram analysis method (WHAM) version 2.0.9 to derive the free energy profiles from the potential of mean forces of the metal probes crossing the TM channel [43]. The standard deviations or error bars in the PMF calculations were derived from both bootstrapping and block analysis but are not reported due to their very small values.

All MD trajectories and umbrella sampling simulations are freely available from the Zenodo website at https://zenodo.org/record/2658142 (DOI: https://doi.org/10.5281/zenodo.2658142).

3. Results

Our model of the *E. coli* YiiP dimer in the inward-facing state was built by merging the model of the TMD built on the cryo-EM structure of the *S. oneidensis* homolog with the higher quality CTD obtained from the outward-facing crystal structure of *E. coli* YiiP (Fig. 1A). The CTD is

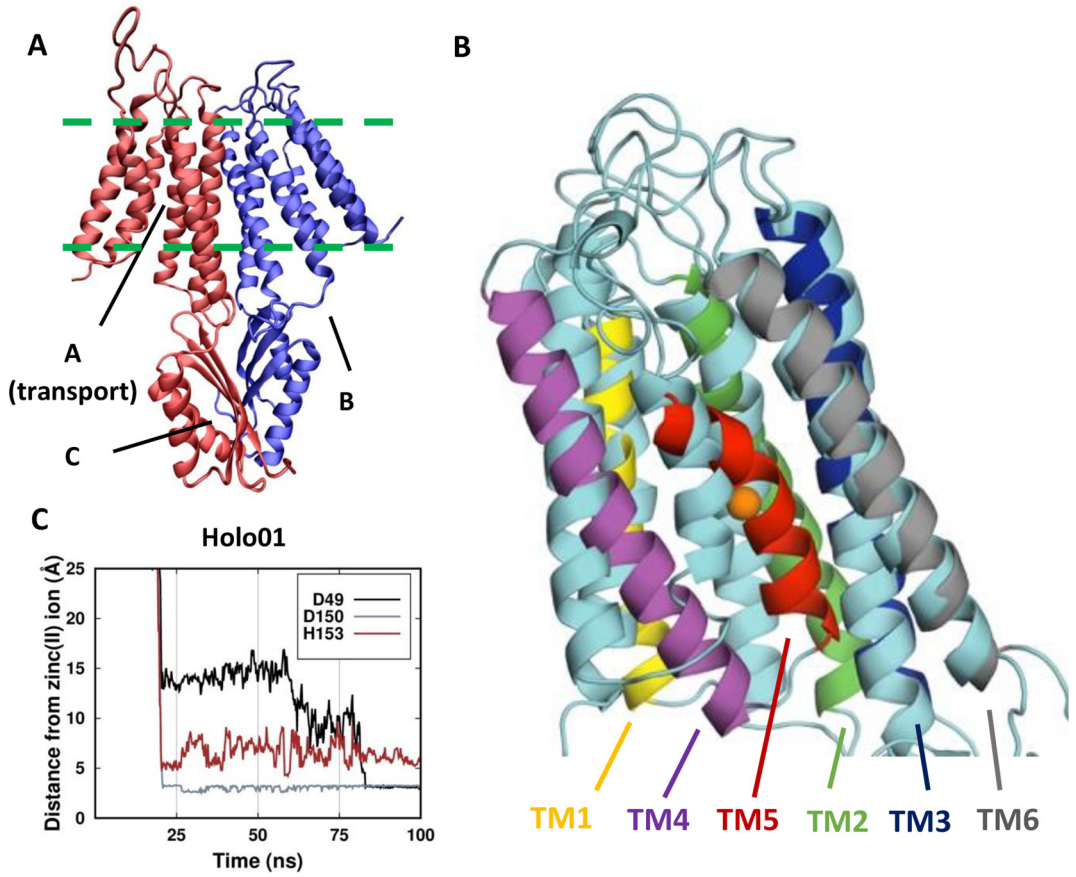

Fig. 1. Model of the *E. coli* YiiP transporter in the inward-facing state. A) The three zinc(II) binding sites are indicated (A-C). The two protein chains are colored differently. B) Fitting of the final snaphot of chain B on the starting conformation in the Holo01 simulation. The starting conformation is in cyan. The zinc(II) ion is shown as an orange sphere. **C)** Zinc(II) interaction pathway in the TM cavity. The distances are measured from the zinc(II) ion to the Cγ atom of D49, D150 and to the Nδ atom of H153. (For interpretation of the references to color in this figure legend, the reader is referred to the web version of this article.)

structurally identical in both the protein states. The resulting dimeric protein model was embedded in a lipid bilayer and solvated (see Methods). Overall, we carried out four classical MD simulations: three in the presence of 0.150 M of $ZnCl_2$ (holo) and one without zinc(II) ions in solution. The two longest holo-simulations started from the same conformation and sampled a trajectory length of 1 μs each. Hereafter, we will refer to these two runs as “Holo01” and “Holo02”. Also the simulation of YiiP in absence of zinc(II) ions (“No-zinc” hereafter) spanned a time length of 1 μs. A further replica of the holo system was performed for 540 ns starting from a snapshot of the “Holo01” run with the zinc(II) ion already bound to the binding site in the channel. We will refer to this replica as “Replica01”. Finally, we performed three umbrella simulations using the zinc(II) (2 runs) and sodium(I) ions as probes to assess the metal-dependent free-energy barriers of the channel permeation process.

3.1. Simulations of Holo-YiiP

In the presence of zinc(II) ions in solution, the final structures of the two Holo trajectories at 1 μs featured both sites B on the IL1 loops (Fig. 1A) populated by zinc(II) ions. More importantly, in both runs one zinc(II) ion entered the transmembrane (TM) cavity. The zinc(II) ion entered the channel of chain B in the Holo01 run as opposed to chain A in the Holo02 run. However, only in Holo01 the zinc(II) ion moved from the TM cavity to the transport site (Fig. 1B), whereas in Holo02 the ion remained stably bound at the entrance of the TM cavity (Fig. S2).

The distances from the residues interacting with the zinc(II) ions in the TM cavities were measured along the simulation (Fig. 1C). In the diffusion process from the cytosol towards the transport site in the Holo01 simulation, the zinc(II) ion interacted mainly with three residues: D150, which is part of the region of the TM5 helix facing the intracellular space, D49, which is part of the transport site on the TM2 helix, and H153, which is part of the transport site on the TM5 helix (Fig. 1B and Movie S1). After binding to the transport site, the zinc(II) ion remained coordinated by D49 and D150 until the end of the simulation.

In the Holo02 simulation the metal ion interacted simultaneously with D150 and E79 at the entrance of the TM cavity (Fig. S3). The latter interaction was not observed in the Holo01 trajectory. Although H153 repeatedly approached the zinc(II) ion in the first half of the simulation, the two negative charges of E79 and D150 produced an electrostatic attraction on the metal ion so strong as to prevent further displacement of the ion towards the TM cavity. To analyze whether the additional carboxylate recruited by the zinc(II) ion in Holo02 with respect to Holo01 was indeed the main responsible for preventing the transit of the cation along the channel, we removed the charge of E79 by replacing it with alanine (E79A mutant) and re-started the simulation. Upon mutation, the metal ion was able to move away from the entrance of the channel and bound to D49 similarly to Holo01 (Fig. S4).

The channel accessibility along time can be estimated by measuring a structural parameter, such as the TM cavity opening, and a biochemical parameter, such as the hydration of the channel. In this work, the channel accessibility was assessed by measuring the distances of the stable TM3 (represented by I90) helix from TM1 (A20), TM2 (D49), TM4 (I130), TM5 (L152) and TM6 (M197) (Fig. 2). In all the holo-

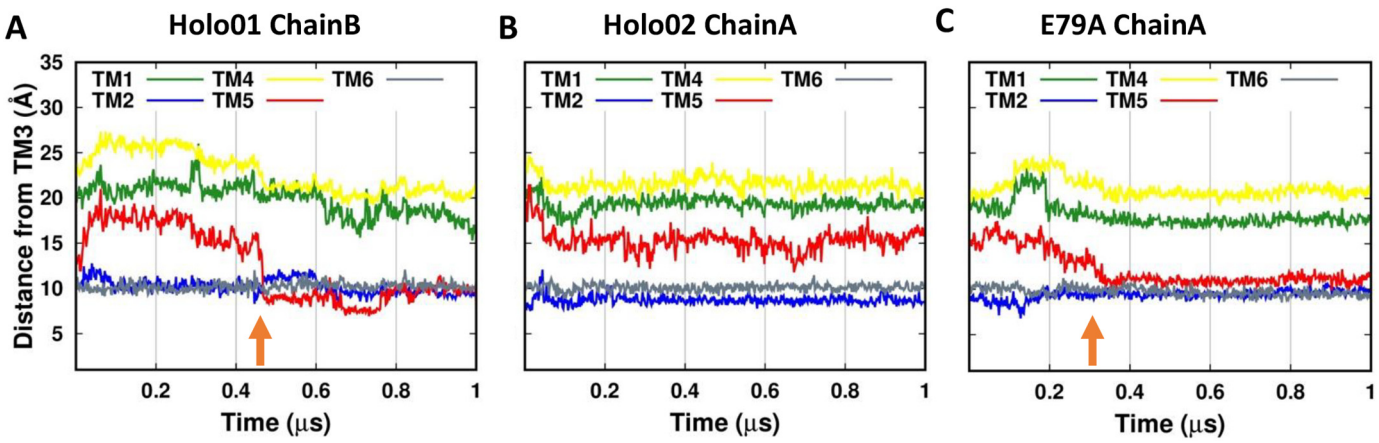

Fig. 2. TM cavity opening and water accessibility as a function of time in Holo01 chain B, Holo02 chain A and mutant E79A chain A, respectively. The graphs show the distances from the Cα atom of I90 in the TM3 helix to the Cα atoms of A20 (TM1), D49 (TM2), I130 (TM4), L152 (TM5) and M197 (TM6). The reorientation of TM5 is marked by an orange arrow.

simulations, TM2 and TM6 showed a very stable behavior preserving a direct contact with TM3. On the contrary, at the beginning of the Holo01 run the chain permeated by the zinc(II) ion displayed a rapid increase of the TM3-TM4 and TM3-TM5 distances followed by a gradual decrease to 15 Å (Fig. 2A). At 470 ns, these distances suddenly dropped due to the reorientation of TM5. In particular, the TM3-TM5 distance reached the same values as TM3-TM2 and TM3-TM6, denoting a direct contact between the TM helices. We can interpret this behavior as the channel being initially in a more exposed (open) configuration, followed by a large-scale rearrangement, induced or stabilized by the presence of the zinc(II) ion in the transport site, that eventually closed the channel. Of note, the Replica01 simulation, where a zinc(II) ion was already bound at the transport site, sampled the same large-scale rearrangement seen in Holo01 (Fig. S5A). Instead, in the chain A of Holo02, where the zinc(II) ion was stably bound at entrance of the TM cavity, all the distance profiles remained fairly constant throughout the whole simulation and did not feature any relevant conformational changes, in what can be regarded as an essentially open configuration (Fig. 2B). Allowing the zinc(II) ion to reach the transport site by restarting the Holo02 run after introducing the E79A mutation resulted in the same reorientation of TM5 observed in Holo01 (Fig. 2C). Furthermore, after this reorientation, the zinc(II) coordination became similar to the tetrahedral geometry of the outward facing configuration for some nanoseconds, with the exception of D150 taking the place of H153 (Fig. S4). This configuration allowed a second zinc(II) ion to approach the site from the extracellular environment, suggesting the existence of an accessible extracellular cavity.

Variations of the channel hydration in response to the conformational motions caused by zinc(II) binding were measured experimentally by Gupta et al. [31]. To obtain a qualitative comparison with these data we measured the time evolution of the number of water molecules (cutoff at 5 Å) surrounding the residues in the TM cavity (Fig. 3). For this analysis, we selected the residues that in experiments displayed the largest response to the presence of zinc(II) ions in solution, namely the average of V48, D49 and I50 (these three residues are grouped together in the experimental work), M151, L152 and M197. The profiles of the V48-D49-I50 group (TM2), L152 (TM5) and M197 (TM6) of chain B displayed a similar trend in the Holo01 and Replica01 simulations (Fig. 3A and S5B). These residues featured the highest water accessibility with TM4 and TM5 far away from TM3. Then, their accessibility dropped when TM5 closed the gap with TM3 closing the channel. Differently from the rest, the water accessibility of M151 (TM5) increased after the channel closed. This effect is more evident in Replica01 and E79A than Holo01. Notably, M151 displayed an opposite trend of experimental hydration change upon zinc(II) exposure with respect to the other residues examined here [31]. For comparison, in the zinc(II)-bound chain A of the Holo02 simulation, V48-D49-I50 and M197 sampled intermediate values between the poorly solvated M151 and the highly solvated L152 (Fig. 3B). Thus, the channel of chain A remained partly accessible from the IC space. The E79A mutant sampled the same TM5 rearrangement as Holo01 and Replica01. However, here only the water accessibility of M197 dropped (Fig. 3C). This is due to the fact that in this simulation a second cavity exposed to the extracellular environment increased the solvation of the top part of the channel.

We then looked at the chains where zinc(II) did not enter the channel. In chain A of Holo01 TM5 sampled short distances from TM3, denoting a TM cavity constantly closed from the IC (Fig. S6A). A similar behavior was observed also for chain B in the Holo02 simulation, with the exception of TM2 being modestly more distant from TM3 (Fig. S6B). Accordingly, the presence of water molecules in the channel was quite low for chain A of Holo01 as well as for chain B of Holo02, with the exception of the V48-D49-I50 triad in the latter simulation (Fig. S6C and S6D).

We monitored the accessibility of the TM cavity also through the distance between the side chains of L152 and M197 (Fig. 4). These residues were always in direct contact in chain A of the Holo01 and Replica01 simulations, corresponding to an inaccessible cavity. On the contrary, for chain B the interaction was suddenly achieved when the channel closed and conserved until the end of the trajectory. The conformational change that closed the channel corresponded to a rotation and tilt of TM5 that brought the L152 side chain in close contact with the side chains of I90 from TM3 and of M197 from TM6 (Movie S2). This interaction created a hydrophobic gate modulating the access of water from the IC space to the TM cavity and in turn to the transport site. The snapshots at 466 ns and 470 ns displaying the top view of the TM cavity on the chain B of Holo01 point out the link between the L152-M197 distance and the presence of water molecules in the cavity (Fig. 5). In particular, the snapshot at 466 ns shows that L152 and M197 were distant enough to allow water/ions to enter the TM cavity from the IC space. In fact, the TM cavity is filled by water molecules. Four ns later, the close contact between the side chains of L152 and M197 prevented the access to the TM cavity from the cytosol. As consequence, the number of water molecules in the cavity dropped. In addition to the above residues, A149 of TM5 approached A83 and I90 of TM3 and to A194 of TM6 making a packed cluster of side chains that reinforced the hydrophobic barrier separating the transport site from the IC space (green sticks in Fig. 5). The time evolution of this hydrophobic cluster closely paralleled the formation of the L152-M197 gate (compare Fig. 4A and Fig. S7).

To obtain further insights into the conformational dynamics of the

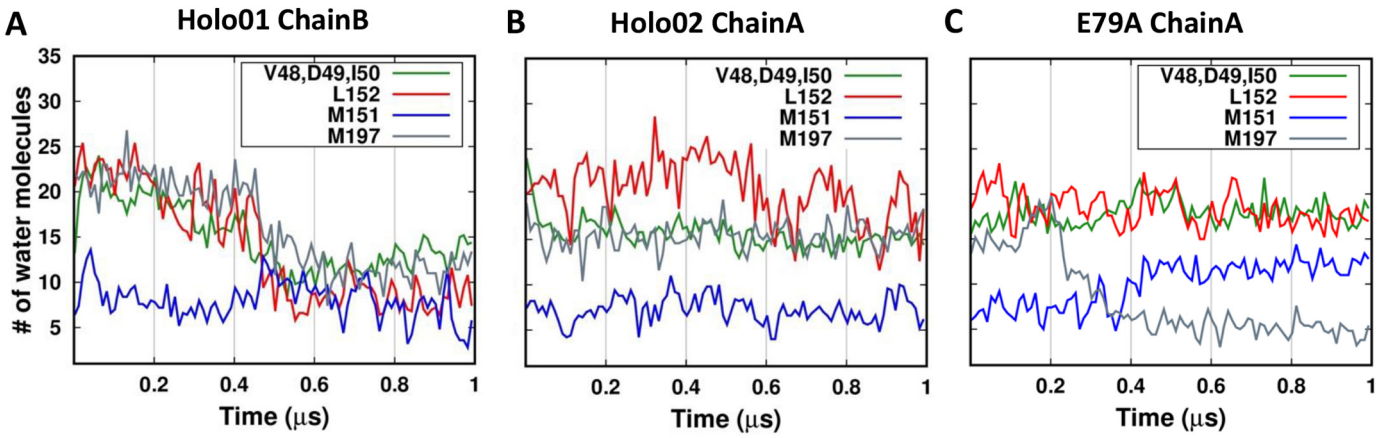

Fig. 3. Number of water molecules within 5 Å from the reported residues in the A) Holo01 chain B, B) Holo02 chain A and C) mutant E79A chain A, respectively.

TM helices in the Holo01 simulation, we calculated the atomic correlation of motions, dividing the whole simulation into two parts: before and after the reorientation of TM5 occurring at 470 ns (Fig. 6). Besides the obvious correlation among residues close in sequence, the loops EL2 (connecting TM3 and TM4) and EL3 (connecting TM5 and TM6) featured the highest correlation during the first 470 ns of simulation (Fig. 6A). This could suggest a sort of communication pathway between the TM3-TM6 helix pair and the TM4-TM5 helices of the four-helix bundle. In the second part of Holo01, the motions of TM5 and the lower part of TM4 were correlated with those of TM3 and TM6 (Fig. 6B). This correlation was absent in the first 470 ns of the simulation. Thus, the reorientation of TM5 linked directly TM4 and TM5 to the TM3-TM6 helix pair.

The principal component analysis (PCA) carried out on the Cα atoms of the Holo01 simulation highlighted the main conformational motions in a few principal components or eigenvectors. In particular, performing the PCA on the TM helices of the Holo01 chain B (excluding the long EC loops) together with the IL1 loop resulted in the first eigenvector containing 62% of the overall motions. The widest motion involved the TM4-TM5 helices (Movie S3), which moved towards the TM3-TM6 helix pair covering a long distance. In this process TM5 not only translated towards the TM3-TM6 helix pair along with TM4, but it also rotated towards the TM cavity as already described in the previous paragraphs. This is accompanied by a smaller-scale reorientation of the TM3-TM6 pair, resulting in a coordinated conformational change that modulates the packing of the four-helix bundle against the TM3-TM6 pair. We then performed a second PCA including also the CTDs (Movie S4). The first eigenvector collected 71% of the overall motions and showed again the main contributions to the mobility given by TM4, TM5 and the IL1 loop. In addition, a rotation of the CTDs was observed, thus suggesting a connection between the CTD dynamics and the conformational changes recorded in the TM region of chain B. Notably, the superposition of the TMDs of the final structures of Holo01 and Holo02 reveals that the two CTDs are tilted in opposite directions (Fig. S8A). In fact, in both structures the CTD tilted towards the chain whose TM cavity was inaccessible. The tilt was greater for the Holo01 run than the Holo02 run, possibly due to the presence of a zinc(II) ion bridging site B (which is located on the IL1 loop) of chain A to the CTD, observed only in Holo01.

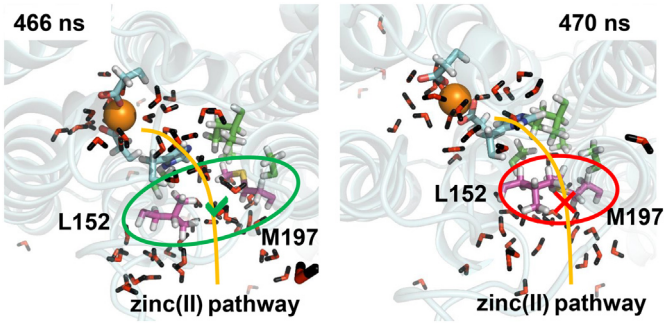

Fig. 5. Top view of the Holo01 chain B channel at 466 and 470 ns. L152 and M197 are depicted as magenta sticks, water molecules are shown as thin sticks. The residues forming the hydrophobic cluster are shown as green sticks. The residues of the transport site coordinating the zinc(II) ion are indicated as cyan sticks. (For interpretation of the references to color in this figure legend, the reader is referred to the web version of this article.)

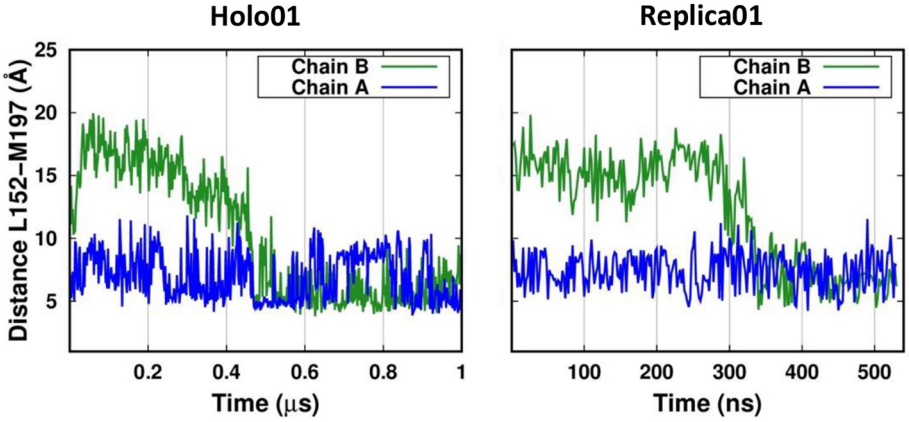

Fig. 4. Hydrophobic gate regulating the access to the TM cavity from the IC space. The distances are measured between the Cγ of L152 and the Cε of M197 in both the protein chains.

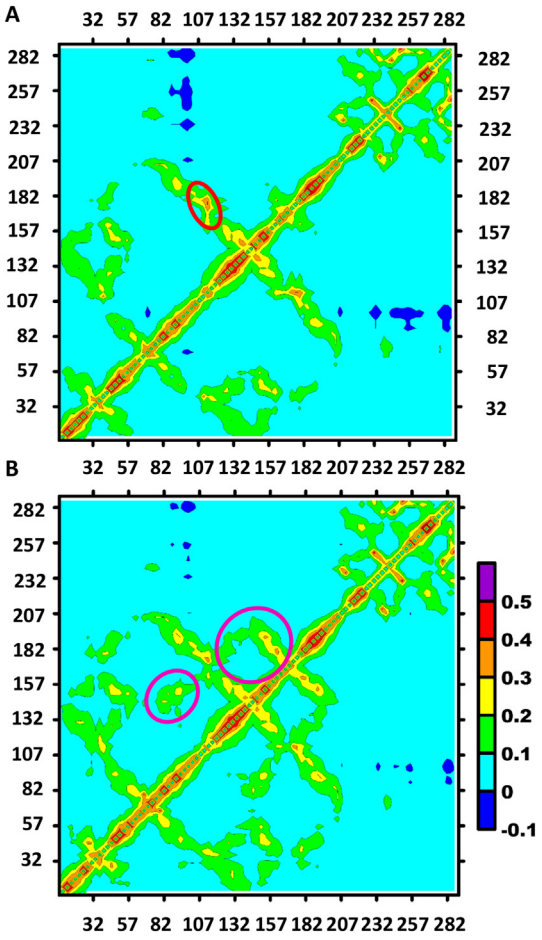

Fig. 6. Residue-residue correlations of the Holo01 Chain B. A) Correlations in the time range 1-470 ns. The red circle indicates the region with the highest correlation. B) Correlations in the time range 471–1000 ns. The magenta circles indicate the regions with correlations arisen in this time range.

3.2. Simulation of YiiP in the absence of zinc(II) ions

The No-zinc simulation was performed without zinc(II) ions in solution for a time sampling of 1 μs. We are aware that using the structure of holo-YiiP as the starting point of the No-zinc run could be far from the correct conformational ensemble sampled by apo-YiiP. Indeed, in this simulation the global structure experienced larger fluctuations than in the Holo-simulations (Fig. S1). However, the main goal of this simulation was to investigate whether the conformational changes featured in the holo simulations are zinc-dependent. To reach this goal we exploited the unique feature of molecular modelling that permits the simulation of non-physiological conditions. Thus, in this simulation a force was applied to prevent the sodium(I) and chloride(I) ions access in the TM cavities, so that the cations could not induce conformational effects similar to zinc(II), while preserving the physiological protein-sodium chloride interactions in the remaining regions of the protein.

To compare with the previous trajectories, we measured the distances of TM3 (I90) from TM1 (A20), TM2 (D49), TM4 (I130), TM5 (L152) and TM6 (M197) as a gauge of the accessibility of the TM cavity (Fig. S9). For chain A, the profile is similar to that observed for chain B of the Holo01 run, consistent with high accessibility of the cavity (Fig. S9A). On the contrary, TM5 in the chain B sampled shorter distances corresponding to the partially accessible or, for short time intervals, inaccessible cavity (Fig. S9B). In accord to this scenario, the L152-M197 distance sampled high values for the chain A and intermediate values for the chain B (Fig. S10). By superimposing the TMDs of the final conformations of the Holo01 and the No-zinc runs, it became apparent that also in this case the CTDs tilted towards the chain whose cavity is inaccessible (chain A of Holo01 and chain B of No-zinc) (Fig. S8B).

3.3. Umbrella simulations

The Holo01 simulation provided us a detailed view of the zinc(II) interactions along the pathway for diffusion towards the transport site. This information can be used to perform a so-called umbrella simulation to derive the free-energy barrier encountered by the ion. The metal dependency of the energetic barriers can be estimated by replacing the zinc(II) ion with other metals. Thus, we performed three umbrella simulations using a zinc(II) or sodium(I) ion as probe on the inward-facing state. The two zinc runs exploited the same starting conformation extracted from the unbiased Holo01 run when the metal ion is located at the entrance of the TM cavity of chain B (corresponding to 0 Å in Fig. 7). Instead, the sodium run started with the ion placed some angstroms away from the channel entrance. The more distant starting point of the sodium(I) than zinc(II) runs is motivated by the fact that there is no evidence in the literature that sodium can enter YiiP. Thus, measuring the energetic barrier of the metal approach to the channel entrance can be relevant. The highest free-energy barrier encountered when moving from the cytosol to the transport site was similar for both metal ions (Fig. 7). In correspondence of the energetic minima, the two metal ions interacted with the same residues (Fig. S11). In particular, the coordination of the zinc(II) ion is the same as in the unbiased Holo01 simulation, with the carboxylates of D150 and D49 interacting with the metal (Fig. S11A). Instead, the energetic profiles when going from the transport site to the EC space differed significantly between the two metals. The sodium(I) ion free-energy increased only slightly before reaching the top of the channel. Instead, in the two zinc(II) runs we observed a dramatic energy increase when detaching from D157 in the transport site to move to the top of the channel. In summary, the inward-facing conformation favored the entrance of the cations in the

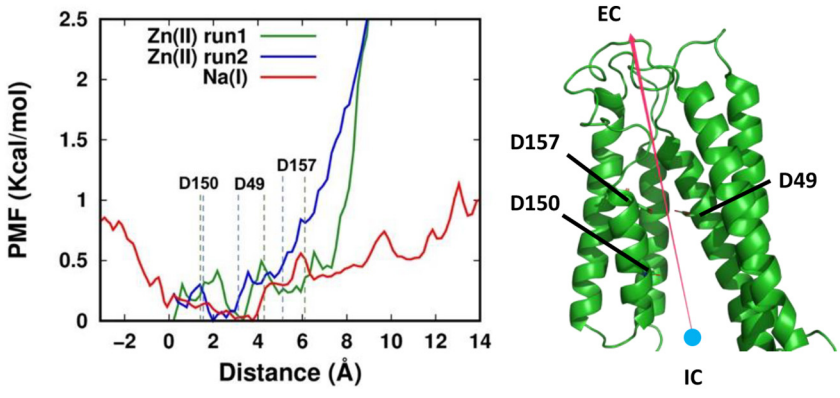

Fig. 7. Free-energy profiles of the zinc(II) and sodium(I) ions crossing the TM cavity. The channel entrance from the IC is aligned at 0 Å. The main binding residues are reported.

TM cavity and their translocation to the transport site. Here, the coordination environment of the zinc(II) ion is well defined; similar interactions with the protein have been observed also for the sodium(I) cation. In the process of release from the transport site, the zinc(II) ion experienced a dramatically high energetic barrier, which effectively prevents its free diffusion from the channel to the bulk solution. This suggests that a significant conformational rearrangement is needed to lower the energetic barrier for the exit of the zinc(II) ion. Interestingly, there is a comparatively much lower barrier for the release of the sodium(I) ion, indicating that the interactions of the latter within the transport site are somewhat weaker, albeit structurally similar, than those formed by the zinc(II) ion. This can be ascribed to the higher charge of the zinc cation.

4. Discussion

The main force that drives the zinc(II) ions towards the YiiP protein channels is electrostatic attraction. Indeed, the YiiP transporter has three negatively charged residues located at the entrance of the TM cavity: E79 on TM3, D150 on TM5 and E200 on TM6. In our holo-simulations the zinc(II) ion permeating the TM cavity bound to D150 or D150 and E79. In particular, the simultaneous interaction with both D150 and E79 occurring in the Holo02 run blocked the metal ion at the TM cavity entrance for the entire simulation. Instead, in the Holo01 run the metal ion interacted initially only with D150, allowing it to subsequently reach the transport site. We thus postulated that the zinc(II) interaction with two negative charges generated a very high energetic barrier preventing the ion from moving deeper in the channel and also inhibiting the rearrangement of TM5. We tested this hypothesis by mutating E79 to alanine. In the E79A mutant, the zinc(II) ion previously blocked at the entrance of the TM cavity reached the transport site as seen in the Holo01 simulation (Fig. S4). Notably, the human homologs of YiiP lack D150, which could result in a similar effect of lowering the energetic barrier for the diffusion of zinc(II) within the channel while preserving the negative electrostatic potential needed for attracting the ions from the IC space [44]. Indeed, the energetic profile of Fig. 7 indicates that once the metal ion has reached the entrance of the TM cavity, its translocation to the transport site encounters modest barriers. Electrostatics is, based on our energetics calculations, a crucial factor also in preventing the free diffusion of the metal ion from the transport site towards the EC space in the inward-facing state of YiiP.

The possibility for the zinc(II) ion to enter the TM cavity from the IC space is related to the accessibility of the TM cavity delimited by the four-helix bundle (TM1, TM2, TM4 and TM5) and the TM3-TM6 helix pair. It has been proposed that the dynamics of TM5 with respect to the TM3-TM6 helix pair is the main factor in modulating the access to the transport site [31]. Our Holo simulations demonstrated a tight correlation between the motion of helices TM5 and, to a lesser extent, TM4 and the presence of water molecules in the TM cavity. The TM helices sampled short distances in the chains not permeated by zinc(II) and had low solvation, corresponding to a closed configuration. Instead, the chains whose TM cavity was permeated by zinc(II) displayed a relevant increase of the distance between the TM4-TM5 pair and the TM3-TM6 pair at the beginning of the simulation (open configuration); this was accompanied by relatively high hydration of the channel (Figs. 2 and 3). After the zinc(II) ion reached the transport site by binding to D49, TM4 and TM5 slowly closed the gap with the TM3-TM6 helix pair. In parallel, the number of water molecules in the cavity gradually decreased. Then, a rapid conformational change took place that put TM5 in close contact with the TM3 making the TM cavity inaccessible from the IC space. The rearrangement of TM5 involved also a motion of TM4, so that the whole structural change can be described as the four-helix bundle achieving a tighter packing against the TM3-TM6 pair. In our Holo01 and Replica01 simulations, this led to the formation of a hydrophobic gate between L152 and M197 (Figs. 4 and 5). This process was highlighted by X-ray–mediated hydroxyl radical labeling measurements, leading to the suggestion that the hydrophobic gate is responsible for the regulation of zinc(II) access to the TM cavity [31]. Our simulations support this view.

In all Holo runs, including the E79A mutant, we found only one of the two available TM cavities was accessible, whereas the other was totally or partially inaccessible. Therefore, the usual symmetric representation of the YiiP transporter does not match the dynamics sampled by our simulations. The open cavity was the one permeated by the zinc(II) ion. In the simulation without zinc(II) ions both chains were in an open or partly open configuration. Thus, it is possible that the binding of zinc(II) initially stabilizes the chain in the open configuration while the other chain rearranges to the closed configuration. Subsequently, when the zinc(II) ion reaches the transport site also the first chain reorganizes to reach the closed configuration.

Based on X-ray–mediated hydroxyl radical labeling measurements, it was suggested that zinc(II) binding at the transport site with tetrahedral coordination geometry is the crucial event to trigger the conformational change of TM5 [31]. In particular, it was hypothesized that this rearrangement would cause the TM cavity to close in the portion facing the IC while opening towards the extracellular side in a sort of alternating mechanism. Here, in the Holo01 and Replica01 simulations YiiP underwent a wide conformational change that caused the closing of the TM cavity upon zinc(II) binding at the transport site. To achieve this, it was sufficient for the zinc(II) ion to reach a stable interaction with only D49 of the transport site, suggesting that tetrahedral coordination is not essential to trigger the reorientation of TM5. Only in the E79A simulation we could observe the coordination sphere of the zinc(II) ion in the transport site achieve a geometry very similar to the tetrahedral geometry of the outward facing configuration. Intriguingly, this event was accompanied by other smaller-scale structural changes, which allowed a second zinc(II) ion to approach the site from the EC side of the protein. This observation is in line with a recent experimental work suggesting that a conformation of the transporter where a persistent dimer interface is combined with an inaccessible intracellular cavity and an accessible extracellular cavity is able to transport zinc(II) across the membrane [29]. Overall, our simulations and the latter experimental data indicate that the four-helix bundle rearranges with respect to a static TM3-TM6 helix pair scaffold, in a rocking-bundle mechanism common also in other active transporters as LeuT [45,46]. This mechanism was apparent in the conformational dynamics sampled in the Holo01 run (Movie S5), even though the simulation length is very short compared to the estimated timescale of the overall zinc(II) transport process [23,47]. Furthermore, our umbrella simulations showed that the IC-facing conformation permitted the translocation of zinc(II) to the transport site but not its release. Thus, we can postulate that a further conformational change involving at least the TM helices harboring the zinc(II)-binding residues (TM2 and TM5) is needed to lower the free-energy barrier of the zinc(II) release process [44].

In conclusion, our simulations combined with the available structural and experimental data on YiiP provide an atomistic view of various steps of the transport mechanism involving the inward-facing conformation. First of all, we observed that during zinc(II) transport the symmetry of the YiiP dimer is lost, with the channels in the two chains consistently featuring a significantly different accessibility. Zinc(II) permeation within the TM cavity of one chain is sufficient to trigger the compaction of the four-helix bundle and the TM3-TM6 helix-pair in the TMD of that chain. After the zinc(II) ion fully enters the transport site further structural changes may put the site in communication with the extracellular space without achieving a full transition of the outward-facing state. Nevertheless, our energy calculations suggest that there is a substantial energetic barrier preventing the release of the ion from the coordination environment in the transport site. Our data do not allow us to evaluate how this barrier is eventually removed, an event which may be combined with the proton antiport performed by YiiP.

Supplementary data to this article can be found online at https://doi.org/10.1016/j.bbagen.2019.06.001.

Acknowledgements

This work was supported by Consorzio Interuniversitario Risonanze Magnetiche di Metallo Proteine (CIRMMP).

References

[1] R.J.P. Williams, J.J.R. Frausto da Silva, The Biological Chemistry of the Elements: The Inorganic Chemistry of Life, Oxford University Press, 2001.
[2] W. Maret, Zinc biochemistry: from a single zinc enzyme to a key element of life, Adv. Nutr. An Int. Rev. J. 4 (2013) 82–91, https://doi.org/10.3945/an.112.003038.
[3] A. Krężel, W. Maret, The biological inorganic chemistry of zinc ions, Arch. Biochem. Biophys. 611 (2016) 3–19, https://doi.org/10.1016/j.abb.2016.04.010.
[4] J.L. Vinkenborg, T.J. Nicolson, E.A. Bellomo, M.S. Koay, G.A. Rutter, M. Merkx, Genetically encoded FRET sensors to monitor intracellular Zn2+homeostasis, Nat. Methods 6 (2009) 737–740, https://doi.org/10.1038/nmeth.1368.
[5] C. Cubillas, P. Vinuesa, M.L. Tabche, A. García-De Los Santos, Phylogenomic analysis of cation diffusion facilitator proteins uncovers Ni_2^+/Co_2^+ transporters, Metallomics. 5 (2013) 1634–1643, https://doi.org/10.1039/c3mt00204g.
[6] B. Montanini, D. Blaudez, S. Jeandroz, D. Sanders, M. Chalot, Phylogenetic and functional analysis of the Cation Diffusion Facilitator (CDF) family: improved signature and prediction of substrate specificity, BMC Genomics 8 (2007) 107, https://doi.org/10.1186/1471-2164-8-107.
[7] S. Barber-Zucker, B. Shaanan, R. Zarivach, Transition metal binding selectivity in proteins and its correlation with the phylogenomic classification of the cation diffusion facilitator protein family, Sci. Rep. 7 (2017) 1–12, https://doi.org/10.1038/s41598-017-16777-5.
[8] H. Zhao, D. Eide, The yeast ZRT1 gene encodes the zinc transporter protein of a high-affinity uptake system induced by zinc limitation, Proc. Natl. Acad. Sci. U. S. A. 93 (1996) 2454–2458, https://doi.org/10.1073/pnas.93.6.2454.
[9] N. Grotz, T. Fox, E. Connolly, W. Park, M.L. Guerinot, D. Eide, Identification of a family of zinc transporter genes from Arabidopsis that respond to zinc deficiency, Proc. Natl. Acad. Sci. 95 (1998) 7220–7224, https://doi.org/10.1073/pnas.95.12.7220.
[10] R.D. Palmiter, L. Huang, Efflux and compartmentalization of zinc by members of the SLC30 family of solute carriers, Pflugers Arch. Eur. J. Physiol. 447 (2004) 744–751, https://doi.org/10.1007/s00424-003-1070-7.
[11] L. Huang, S. Tepaamorndech, The SLC30 family of zinc transporters-a review of current understanding of their biological and pathophysiological roles, Mol. Asp. Med. 34 (2013) 548–560, https://doi.org/10.1016/j.mam.2012.05.008.
[12] O. Kolaj-Robin, D. Russell, K.A. Hayes, J.T. Pembroke, T. Soulimane, Cation diffusion facilitator family: structure and function, FEBS Lett. 589 (2015) 1283–1295, https://doi.org/10.1016/j.febslet.2015.04.007.
[13] I.T. Paulsen, M.H. Saier, A novel family of ubiquitous heavy metal ion transport proteins, J. Membr. Biol. 156 (1997) 99–103, https://doi.org/10.1007/s002329900192.
[14] A. Salusso, D. Raimunda, Defining the roles of the Cation diffusion facilitators in Fe^{2+}/Zn^{2+} homeostasis and establishment of their participation in virulence in *Pseudomonas aeruginosa*, Front. Cell. Infect. Microbiol. 7 (2017) 1–14, https://doi.org/10.3389/fcimb.2017.00084.
[15] E. Bafaro, Y. Liu, Y. Xu, R.E. Dempski, The emerging role of zinc transporters in cellular homeostasis and cancer, Signal Transduct. Target. Ther. 2 (2017) 17029, , https://doi.org/10.1038/sigtrans.2017.29.
[16] T. Kambe, Y. Yamaguchi-Iwai, R. Sasaki, M. Nagao, Overview of mammalian zinc transporters, Cell. Mol. Life Sci. 61 (2004) 49–68, https://doi.org/10.1007/s00018-003-3148-y.
[17] G. Grass, M. Otto, B. Fricke, C.J. Haney, C. Rensing, D.H. Nies, D. Munkelt, FieF (YiiP) from Escherichia coli mediates decreased cellular accumulation of iron and relieves iron stress, Arch. Microbiol. 183 (2005) 9–18, https://doi.org/10.1007/s00203-004-0739-4.
[18] Y. Wei, H. Li, D. Fu, Oligomeric state of the *Escherichia coli* metal transporter YiiP, J. Biol. Chem. 279 (2004) 39251–39259, https://doi.org/10.1074/jbc.M407044200.
[19] D.S. Parsons, C. Hogstrand, W. Maret, The C-terminal cytosolic domain of the human zinc transporter ZnT8 and its diabetes risk variant, FEBS J. 285 (2018) 1237–1250, https://doi.org/10.1111/febs.14402.
[20] R. Sladek, G. Rocheleau, J. Rung, C. Dina, L. Shen, D. Serre, P. Boutin, D. Vincent, A. Belisle, S. Hadjadj, B. Balkau, B. Heude, G. Charpentier, T.J. Hudson, A. Montpetit, A.V. Pshezhetsky, M. Prentki, B.I. Posner, D.J. Balding, D. Meyre, C. Polychronakos, P. Froguel, A genome-wide association study identifies novel risk loci for type 2 diabetes, Nature. 445 (2007) 881–885, https://doi.org/10.1038/nature05616.
[21] G.A. Rutter, F. Chimienti, SLC30A8 mutations in type 2 diabetes, Diabetologia. 58 (2015) 31–36, https://doi.org/10.1007/s00125-014-3405-7.
[22] B. Yi, G. Huang, Z. Zhou, Different role of zinc transporter 8 between type 1 diabetes mellitus and type 2 diabetes mellitus, J. Diabetes Investig. 7 (2016) 459–465, https://doi.org/10.1111/jdi.12441.
[23] Y. Chao, D. Fu, Kinetic study of the Antiport mechanism of an Escherichia coli zinc transporter, ZitB, J. Biol. Chem. 279 (2004) 12043–12050, https://doi.org/10.1074/jbc.M313510200.
[24] Y. Wei, D. Fu, Selective metal binding to a membrane-embedded aspartate in the *Escherichia coli* metal transporter YiiP (FieF), J. Biol. Chem. 280 (2005) 33716–33724, https://doi.org/10.1074/jbc.M506107200.
[25] M. Lu, D. Fu, Structure of the zinc transporter YiiP, Science (80-) 317 (2007) 1746–1748, https://doi.org/10.1126/science.1143748.
[26] M. Lu, J. Chai, D. Fu, Structural basis for autoregulation of the zinc transporter YiiP, Nat. Struct. Mol. Biol. 16 (2009) 1063–1067, https://doi.org/10.1038/nsmb.1662.
[27] N. Coudray, S. Valvo, M. Hu, R. Lasala, C. Kim, M. Vink, M. Zhou, D. Provasi, M. Filizola, J. Tao, J. Fang, P.A. Penczek, I. Ubarretxena-Belandia, D.L. Stokes, Inward-facing conformation of the zinc transporter YiiP revealed by cryoelectron microscopy, Proc. Natl. Acad. Sci. U. S. A. 110 (2013) 2140–2145, https://doi.org/10.1073/pnas.1215455110.
[28] O. Jardetzky, Simple allosteric model for membrane pumps, Nature. 211 (1966) 969–970, https://doi.org/10.1038/211969a0.
[29] M.L. Lopez-Redondo, N. Coudray, Z. Zhang, J. Alexopoulos, D.L. Stokes, Structural basis for the alternating access mechanism of the cation diffusion facilitator YiiP, Proc. Natl. Acad. Sci. (2018) 201715051, , https://doi.org/10.1073/pnas.1715051115.
[30] Y. Shi, Common folds and transport mechanisms of secondary active transporters, Annu. Rev. Biophys. 42 (2013) 51–72, https://doi.org/10.1146/annurev-biophys-083012-130429.
[31] S. Gupta, J. Chai, J. Cheng, R. D'Mello, M.R. Chance, D. Fu, Visualizing the kinetic power stroke that drives proton-coupled zinc(II) transport, Nature. 512 (2014) 101–104, https://doi.org/10.1038/nature13382.
[32] N. Eswar, B. Webb, M.A. Marti-Renom, M.S. Madhusudhan, D. Eramian, M. Shen, U. Pieper, A. Sali, Comparative Protein Structure Modeling Using MODELLER, Curr. Protoc. Protein Sci, John Wiley & Sons, Inc, Hoboken, NJ, USA, 2007, pp. 2.9.1–2.9.31, , https://doi.org/10.1002/0471140864.ps0209s50.
[33] E.L. Wu, X. Cheng, S. Jo, H. Rui, K.C. Song, E.M. Dávila-Contreras, Y. Qi, J. Lee, V. Monje-Galvan, R.M. Venable, J.B. Klauda, W. Im, CHARMM-GUI membrane builder toward realistic biological membrane simulations, J. Comput. Chem. 35 (2014) 1997–2004, https://doi.org/10.1002/jcc.23702.
[34] S. Jo, T. Kim, V.G. Iyer, W. Im, CHARMM-GUI: a web-based graphical user interface for CHARMM, J. Comput. Chem. 29 (2008) 1859–1865, https://doi.org/10.1002/jcc.20945.
[35] P. Li, B.P. Roberts, D.K. Chakravorty, K.M. Merz, Rational design of particle mesh Ewald compatible Lennard-Jones parameters for + 2 metal cations in explicit solvent, J. Chem. Theory Comput. 9 (2013) 2733, https://doi.org/10.1021/ct400146w.
[36] R. Gould, I.R. Skjevik, A.A. Dickson, C.J. Madej, B.D. Walker, Lipid17: A Comprehensive AMBER Force Field for the Simulation of Zwitterionic and Anionic Lipids, (2018) In Prep.
[37] J.A. Maier, C. Martinez, K. Kasavajhala, L. Wickstrom, K.E. Hauser, C. Simmerling, ff14SB: improving the accuracy of protein side chain and backbone parameters from ff99SB, J. Chem. Theory Comput. 11 (2015) 3696–3713, https://doi.org/10.1021/acs.jctc.5b00255.
[38] D.A. Case, T.E. Cheatham, T. Darden, H. Gohlke, R. Luo, K.M. Merz, A. Onufriev, C. Simmerling, B. Wang, R.J. Woods, The Amber biomolecular simulation programs, J. Comput. Chem. 26 (2005) 1668–1688, https://doi.org/10.1002/jcc.20290.
[39] D.A. Case, I.Y. Ben-Shalom, S.R. Brozell, D.S. Cerutti, T.E.I. Cheatham, V.W.D. Cruzeiro, T.A. Darden, R.E. Duke, D. Ghoreishi, M.K. Gilson, H. Gohlke, A.W. Goetz, D. Greene, R. Harris, N. Homeyer, S. Izadi, A. Kovalenko, T. Kurtzman, T.S. Lee, S. LeGrand, P. Li, J. Liu, T. Luchko, R. Luo, D.J. Mermelstein, K.M. Merz, Y. Miao, G. Monard, C. Nguyen, H. Nguyen, I. Omelyan, A. Onufriev, F. Pan, R. Qi, D.R. Roe, A. Roitberg, C. Sagui, S. Schott-Verdugo, J. Shen, C.L. Simmerling, J. Smith, J. Swails, R.C. Walker, J. Wang, H. Wei, R.M. Wolf, X. Wu, L. Xiao, D.M. York, P.A. Kollman, AMBER 2018, (2018).
[40] J.F. Nagle, Area/lipid of bilayers from NMR, Biophys. J. 64 (1993) 1476–1481, https://doi.org/10.1016/S0006-3495(93)81514-5.
[41] R. Salomon-Ferrer, A.W. Götz, D. Poole, S. Le Grand, R.C. Walker, Routine microsecond molecular dynamics simulations with Amber on Gpus. 2. Explicit solvent particle mesh Ewald, J. Chem. Theory Comput. 9 (2013) 3878, https://doi.org/10.1021/ct400314y.
[42] B. Roux, The calculation of the potential of mean force using computer simulations, Comput. Phys. Commun. 91 (1995) 275–282, https://doi.org/10.1016/0010-4655(95)00053-I.
[43] M. Andrec, The Weighted Histogram Analysis Method (WHAM), Spring, 2010, https://doi.org/10.1136/bmj.39349.437442.43.
[44] Y. Golan, R. Alhadeff, F. Glaser, A. Ganoth, A. Warshel, Y.G. Assaraf, Demonstrating aspects of multiscale modeling by studying the permeation pathway of the human ZnT2 zinc transporter, PLoS Comput. Biol. 14 (2018) e1006503, , https://doi.org/10.1371/journal.pcbi.1006503.
[45] G. Jeschke, A comparative study of structures and structural transitions of secondary transporters with the LeuT fold, Eur. Biophys. J. 42 (2013) 181–197, https://doi.org/10.1007/s00249-012-0802-z.
[46] L.R. Forrest, G. Rudnick, The rocking bundle: a mechanism for ion-coupled solute flux by symmetrical transporters, Physiology. 24 (2009) 377–386, https://doi.org/10.1152/physiol.00030.2009.
[47] Y. Chao, D. Fu, Thermodynamic studies of the mechanism of metal binding to the *Escherichia coli* zinc transporter YiiP, J. Biol. Chem. 279 (2004) 17173–17180, https://doi.org/10.1074/jbc.M400208200.